Chemical and Biological Technologies in Agriculture

RESEARCH

Open Access

Structural characterization and in vitro hypolipidemic and hypoglycemic activities of a novel neutral polysaccharide from *Siraitia grosvenorii* (Luo Han Guo) flowers

Hao Teng[1,2,3*], Limei Qiu[1], Zhizhi Huang[1], Sam Al-Dalali[1,2,3*], Cailin Li[1,2,3], Aiying Xu[1,2,3] and Zhigui He[1,2,3*]

Abstract

Siraitia grosvenorii, commonly known as Luo Han Guo, is a medicinal and edible plant whose flowers contain bioactive polysaccharides with underexplored therapeutic potential. This study isolated a novel polysaccharide fraction (SGFP-2) from *Siraitia grosvenorii* flowers through DEAE-Crystarose Fast Flow chromatography. Structural analysis revealed SGFP-2 is a heteropolysaccharide with average molecular weight of 1.67×10^5 Da and composed of Rha, Glc, Gal, GlcA, GalA, Man, and Ara with a molar ratio of 8.17:1.54:60.06:3.41:5.37:3.54:15.44. Methylation analysis identified dominant glycosidic linkages of SGFP-2 as →6)-Gal*p*-(1 → (30.42%), Gal*p*-(1 → (22.69%), Ara*f*-(1 → (18.29%), Rha*p*-(1 → (8.70%), → 3,6)-Gal*p*-(1 → (8.54%). Scanning electron microscopy and Congo red staining results showed that the network structure of SGFP-2 was lamellar without trihelix conformation. In vitro experiments have revealed that SGFP-2 possesses lipid-binding capacity, bile salt adsorption properties, and potent inhibitory activity against crucial enzymes involved in glucose-lipid metabolism, specifically pancreatic lipase, cholesterol esterase, α-amylase, and α-glucosidase. These findings suggest that SGFP-2 demonstrates potential hypolipidemic and hypoglycemic effects in vitro. This study provides preliminary evidence to support further development and utilization of *Siraitia grosvenorii* flower polysaccharides.

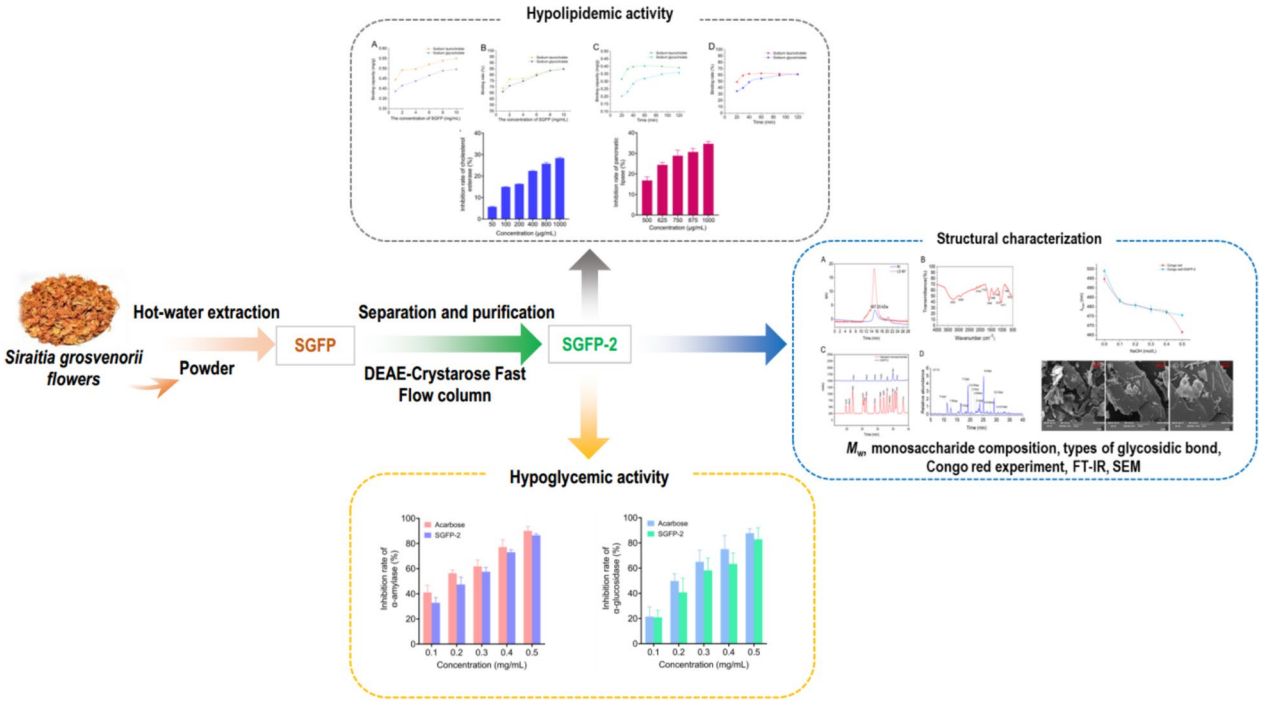
Keywords *Siraitia grosvenorii* flower, Polysaccharides, Structural characterization, Hypoglycemic activity, Hypolipidemic activity

*Correspondence:
Hao Teng
tenghao0557@163.com
Sam Al-Dalali
salihsam4@gmail.com
Zhigui He
hzg@gltu.edu.cn
Full list of author information is available at the end of the article

Springer Open

© The Author(s) 2025. **Open Access** This article is licensed under a Creative Commons Attribution 4.0 International License, which permits use, sharing, adaptation, distribution and reproduction in any medium or format, as long as you give appropriate credit to the original author(s) and the source, provide a link to the Creative Commons licence, and indicate if changes were made. The images or other third party material in this article are included in the article's Creative Commons licence, unless indicated otherwise in a credit line to the material. If material is not included in the article's Creative Commons licence and your intended use is not permitted by statutory regulation or exceeds the permitted use, you will need to obtain permission directly from the copyright holder. To view a copy of this licence, visit http://creativecommons.org/licenses/by/4.0/.

Graphical Abstract



Introduction

Abnormalities in blood lipid and glucose homeostasis are recognized as pivotal drivers of metabolic syndrome and are strongly associated with the pathogenesis of hyperlipidemia, obesity, and type 2 diabetes mellitus [1–3]. Although conventional pharmacological agents, such as statins and sulfonylureas effectively regulate lipid and glucose levels, their long-term toxic side effects and the emergence of drug resistance necessitate the exploration of safer alternatives [4, 5]. This therapeutic impasse has catalyzed interest in plant-derived bioactive compounds with multitarget modulatory capabilities, high safety, and biocompatibility. Among the various strategies being explored for the management of dyslipidemia and hyperglycemia, active compounds of plant origin, particularly polysaccharides, are increasingly recognized as promising candidates for clinical, functional supplementation, and drug development [6, 7]. Encouragingly, recent advances in multi-omics technologies have elucidated the bidirectional crosstalk between gut microbiota dysbiosis and impaired lipid/glucose metabolism, establishing novel therapeutic paradigms for polysaccharide interventions [8, 9].

Siraitia grosvenorii (Luo Han Guo), a dual-purpose medicinal-edible plant endemic to southern China, is primarily cultivated in Guangxi, Guangdong, Guizhou, and Hunan provinces [10, 11]. Flowers, as one of the essential components of *Siraitia grosvenorii* (*S. grosvenorii*), are rich in bioactive compounds [12]. *Siraitia grosvenorii* flowers are valued not only as functional tea ingredients but also as key components in nutraceutical formulations, including herbal decoctions and medicinal porridges. Howerer, current research has disproportionately focused on fruit-derived compounds, creating a knowledge gap regarding the pharmacological potential of phytochemicals in *S. grosvenorii* flowers, especially polysaccharide [13–17]. Recent studies have shown that natural polysaccharides extracted from flowers have considerable potential for application in the development of functional foods due to their unique structure and significant biological activities [18]. Paradoxically, the structural heterogeneity of *S. grosvenorii* flower polysaccharides and the paucity of biological function data severely constrain their industrial applications in functional foods and phytopharmaceuticals.

In this study, a novel neutral polysaccharide was obtained from *S. grosvenorii* flowers by hot water extraction and DEAE-Crystarose Fast Flow column chromatography. Structural characterization using GPC, FT-IR, GC–MS, and SEM revealed key features of

polysaccharide. Finally, the in vitro model was used to evaluate the potential of hypolipidemic and hypoglycemic activities of *S. grosvenorii* flower polysaccharides. This study correlates the structural characteristics of *S. grosvenorii* flower polysaccharides with their experimentally observed biological activities, generating basic data to support further exploration of their therapeutic applications in metabolic regulation.

Materials and methods

Materials and reagents

The flower of *Siraitia grosvenorii* was obtained from Longsheng County, Guilin, Guangxi province, China. DEAE-Crystarose Fast Flow column was purchased from Wuhan Jingcheng Biotechnology Co., Ltd. (Wuhan, China). Ribose, Mannose, Rhamnose, Glucose, Fucose, Galactose, Galacturonic acid, Xylose, Glucuronic acid, Arabinose, and Mannuronic acid were purchased from Sigma Chemical Co., Ltd. (MO, USA). Sodium taurocholate and sodium glycocholate were purchased from Sangon Biotech Co., Ltd. (Shanghai, China). Unless otherwise noted, other additional chemicals and reagents used are analytical quality.

Isolation and purification of polysaccharides

The flowers of *Siraitia grosvenorii* were dried and ground into a powder. The collected residue was extracted using distilled water (1:100, g/mL) at 90 °C for 1 h with continuous stirring. The extraction was conducted thrice, then the filtrate was passed through four layers of gauze, and the filtrates were combined. The filtrate was then concentrated under vacuum at 58 °C, precipitated with ethanol to a final concentration of 80% (v/v) for 24 h at 4 °C, followed by centrifugation at 5000 rpm for 15 min to yield the crude polysaccharide extract. AB-8 macroporous adsorbent resin was mixed with the filtrate in a conical flask and subjected to shaking at 200 r/min for 12 h to facilitate the removal of the pigment. The crude extracts were deproteinized by the Sevag method and dialyzed by a 3000-Da dialysis bag for 72 h. Then, polysaccharide SGFP (*Siraitia grosvenorii* flower polysaccharide) was obtained by vacuum freeze-drying for 48 h. SGFP was fully dissolved in distilled water (20 mg/mL) and centrifuged at 5000 rpm for 15 min. Subsequently, the supernatant was then subjected to a DEAE-Crystarose Fast Flow column (3.6 cm × 50 cm) and eluted with distilled water and NaCl solution (0.1–0.3 mol/L, 2.5 mL/min) to collect three polysaccharide fractions (SGFP-1, SGFP-2, and SGFP-3). The major fraction (SGFP-2) was collected from the 0.2 M NaCl solution eluent.

Structural characterization of SGFP-2

Molecular weight (M_w) analysis

The M_w of SGFP-2 was measured by gel permeation chromatography (GPC) [19]. The polysaccharide sample was first dissolved in 0.1 M $NaNO_3$ (containing 0.02% NaN_3) mobile phase, and then passed through a 0.45-μm filter membrane after dissolution by shaking at 80 ℃; the separation was carried out at a flow rate of 1 mL/min under the column temperature of 40 ℃, and monitored in real time by a detection system; a log(M_w)-retention time calibration curve was established using a narrowly distributed dextran standard ($R^2 > 0.998$) and the absolute molecular weights (M_w, M_n and dispersion) were calculated, and the column efficiency and injection repeatability (RSD < 0.5%) were also verified to finally obtain the molecular weight distribution data.

Chromatographic conditions: Shodex OHpak series SB-806 string 803 column, SEDEX 75 evaporative light scattering detector, mobile phase consisting of H_2O/NaN_3, column temperature kept at 40 °C, with an injection volume of 100 μL and a flow rate of 1 mL/min.

Fourier transform infrared spectroscopy (FT-IR) analysis

The samples were mixed with KBr, and the FT-IR spectra were determined on the Nicolet 6700 FT-IR spectrometer (Thermo Electron, Madison, WI, USA). The sample was scanned in the range of 4000–500 cm^{-1}.

Monosaccharide composition analysis

Monosaccharide compositions of SGFP-2 were determined by HPLC [20]. Accurately weigh an appropriate amount of sample and place it in a hydrolysis tube. Add 1 mL of 72% sulfuric acid and incubate for 1 h in a water bath at 30 °C. Make up the final volume to 10 mL, blow dry with nitrogen, and hydrolyze in an oven at 110 °C for 2 h. Once cooled to ambient temperature, transfer 0.5 mL to a centrifuge tube (4 mL), adjust the pH to neutral, and then make a final volume of 1 mL. Add 0.2 mL of 0.3 mol/L NaOH and 0.4 mL of 3-Methyl-1-phenyl-2-pyrazolin-5-one methanol solution, purge with nitrogen, and incubate in water bath at 70 °C for 60 min. Once cooled to ambient temperature, add 0.2 mL HCl (0.3 mol/L) and dilute with water to a final volume of 2 mL. Add 1.5 mL of chloroform, vortex to mix, allow the layers to separate, and discard the lower chloroform layer. Filter the aqueous layer through a 0.45-μm membrane filter, and then proceed with the HPLC analysis.

Conditions for HPLC analysis: Thermo C18 column (4.6 × 250 mm, 5 μm) and a mobile phase of 0.1 mol/L phosphate buffer solution (pH 6.8) and acetonitrile in a ratio of 83:17 (v/v) were used. The column was kept at a

temperature of 25 ℃, with a flow rate of 1.0 mL/min and an injection volume of 20 μL, and the detection wavelength was set to 254 nm.

Methylation analysis

Methylation analysis is an important tool for structural analysis of polysaccharides [21]. Lyophilized samples were dissolved in 500 μL of DMSO inside a 10-mL hydrolysis tube. Then, the nitrogen was introduced into hydrolysis tube, and the mixture was sonicated for 30 min to solubilize the sample. Then, 10 mg of NaOH powder was added, purged with nitrogen, incubated for 30 min, and cooled the sample in an ice bath until the solution solidified. Purge again with nitrogen, add 0.1 mL of CH_3I, and react for 30 min while maintaining the water bath temperature between 18 °C and 20 °C throughout incubation. The ice bath was cooled until the sample solution was solidified and filled with nitrogen. Then, 0.1 mL of CH_3I was added, and the reaction was carried out for 30 min. The methylation reaction was terminated by adding 1 mL of 4 mmol/L $Na_2S_2O_3$ in water. Subsequently, 1 mL of chloroform was added to the reaction solution, followed by vortex mixing. The mixture was allowed to stand and stratify, after which the lower chloroform phase was obtained. This extraction process was repeated 4 times. Then, the chloroform phases were collected, 1 mL of water was added and centrifuged. The aqueous phase was removed and repeated 4 times. The filtrate was collected and dried by blowing a stream of nitrogen. Following hydrolysis, reduction, and acetylation, the dichloromethane phase was collected and filtered by a 0.45-μm membrane using the machine [22].

The filtrate was analyzed using a 7890B gas chromatograph (Agilent Inc. CA, USA). The injection volume was set at 1 μL, the split ratio was 10:1, and the carrier gas used was high-purity helium; the initial temperature was 50 ℃, held for 1.0 min, and then ramped up to 215 ℃ with a program of 40 ℃/min, and held for mass spectrometry system (Agilent 7000D; Agilent Technologies, USA), equipped with an EI and a MassHunter workstation. The analytes were tested in full scan mode using an EI with a mass scan range (m/z) of 30–600.

Scanning electron microscopy (SEM)

The apparent morphology of SGFP-2 was observed by SEM [23, 24]. After freeze-drying, SGFP-2 was sprayed with gold using an IB-3 ion coating machine. Fix the prepared SGFP-2 on the sample platform and observe the solid morphology of SGFP-2 using SEM (JSM-840, JEOL, Japan) at an acceleration voltage of 20 kV, and the corresponding magnification rates were 200×, 500×, and 1000×, respectively.

Staining with congo red (CR)

The triple-helix structure of polysaccharides was determined using the CR test [25]. A polysaccharide solution (1 mg/mL) was combined with a CR solution at 80 μmol/L in a 1:1 ratio. Subsequently, 2 mL of varying concentrations of NaOH (0 to 1 mol/L) were added, resulting in NaOH (0, 0.1, 0.2, 0.3, 0.4, and 0.5 mol/L). A mixed solution without the polysaccharide served as a control. The reaction was conducted for 10 min under light-avoidance conditions, followed by measuring the maximum absorption wavelength within the 400 to 600 nm range.

In vitro hypolipidemic activity assay

Fat absorption capacity analysis

The fat absorption capacity of polysaccharides was measured following the method described by Yang et al. [26], with minor modifications. A 2 g of SGFP-2 was weighed, and 16 g of edible oil was added. The commixture was incubated at 37 ℃ for 1 h, centrifuged at 4000 rpm for 20 min, discarded the upper layer of oil, and dried residual edible oil in the centrifuge tube. The fat absorption capacity was calculated using Eq. (1)

$$\text{Oil absorption (g/g)} = (M2 - M1)/M1 \quad (1)$$

where M2 is the weight after oil absorption and M2 the weight of the sample.

Sodium cholate adsorption capacity

Sodium cholate adsorption capacity was determined using the previous described method [27]. 3 mL of polysaccharide solutions (1, 2, 4, 6, 8, 10 mg/mL) was placed in a 100-mL conical flask. Subsequently, 3 mL of pepsin (3000 U/mg) and 1 mL of hydrochloric acid solution (0.01 mol/L, pH = 2) were introduced. Digestion occurred via constant temperature oscillation at 37 °C for 1 h. Then, for simulating intestinal environment, the pH was adjusted to 6.3, followed by adding 4 mL of trypsin (250 U/mg), with further digestion conducted under the same conditions for an additional 1 h. Then, 4 mL of bile salt solution was added into each bottleand shaken at 37℃ for 1 h, and then the commixture was transferred into centrifuge tubes and centrifuged at 4000 rpm for 10 min to obtain the supernatant. 1.25 mL of the collected supernatant was mixed with 3.75 mL of 60% sulfuric acid. The mixture was incubated in a water bath at 70 ℃ for 20 min and then transferred into an ice bath for 5 min. The absorbance was measured at 387 nm, and the bile acid salt content was calculated for the sample solution using the standard curve. The binding rates of sodium glycolinate and

sodium taurocholate were calculated using Eqs. (2) and (3), respectively.

$$\text{Sodium glycolinate binding rate}(\%) = \frac{A1 - R1}{A1} \times 100\% \quad (2)$$

$$\text{Sodium taurocholate binding rate}(\%) = \frac{A2 - R2}{A2} \times 100\% \quad (3)$$

where A1 is the addition of sodium glycochenidate, R1 the residual of sodium glycocholate residual, A2 the addition of sodium taurocholate, and R2 the residual of sodium taurocholate.

Adsorption kinetics of cholate

To determine the interaction of polysaccharides with bile acid salts, a sample containing 50 mg of polysaccharide was prepared and supplemented with 4 mL of bile acid salt solution, as delineated in Sect. "Sodium cholate adsorption capacity". The mixture was incubated at a temperature of 37 ℃ for 20, 30, 40, 60, 90, and 120 min, respectively. Following incubation, the samples were centrifuged at a rotational speed of 4000 rpm for a duration of 20 min to sediment any particulate matter. The supernatant was then carefully obtained for further analysis. The concentration of bile salt in the supernatant was subsequently quantified employing the analytical procedure outlined in Sect. "Sodium cholate adsorption capacity". This methodology allows for the assessment of the binding affinity and capacity of the polysaccharide toward bile acid salts under the specified conditions.

Inhibitory effect of SGFP-2 on pancreatic lipase

The inhibitory effect of SGFP-2 on pancreatic lipase was assessed using the method described by Long et al. [28], with minor modifications. 0.05 mL of polysaccharide solution (50, 100, 200, 400, 800, 1000 μg/mL) was pipetted and mixed with 0.05 mL of enzyme solution (20 μg/mL) and 1 mL of phosphate buffer (PB), respectively, and kept at 25 °C for 10 min. Then 0.02 mL of P-Nitrophenyl Butyrate solution (4 mmol/L) was added, reacted at 25 °C for 30 min, and then stood for 10 min. Finally, the absorbance value was assessed at 405 nm. The pancreatic lipase inhibition rate was calculated using formula (4):

$$\text{Inhibition rate}(\%) = [(A1 - A2) - (A3 - A4)]/(A1 - A2) \times 100\% \quad (4)$$

where A1 is the blank tube, A2 the blank control tube, A3 the sample tube, and A4 the sample control tube.

Inhibitory effect of SGFP-2 on cholesterol esterase

The inhibitory effect on cholesterol esterase was evaluated using the method outlined by Long et al. [28], with several modifications. 5 mL of PB solution with a concentration of 0.025 mol/L at pH 7.4 and 1 mL of olive oil were added to the conical flask, followed by a water bath at 37 °C for 5 min. Sequential additions of 25 mg/mL *Siraitia grosvenorii* polysaccharide solution were made to the sample tubes in volumes of 0, 20, 25, 30, 35, and 40 μL. The samples were then incubated in a water bath at 37 °C for 5 min, alongside an untreated control. 1 mL of a 2-mg/mL pancreatic lipase solution was added to the blank tube, and the blank control tube was replaced with ultrapure water. Additionally, 1 mL of the pancreatic lipase solution was added to each sample tube, while a sample blank control was also prepared using ultrapure water instead of the pancreatic lipase solution. The reaction was conducted for 5 min at 37 ℃, after which 15 mL of 95% ethanol was added to each tube to terminate the enzyme reaction. The cholesterol esterase inhibition rate was calculated using formula (5):

$$\text{Inhibition rate}(\%) = [B1 - B2 - (B3 - B4)]/(B1 - B2) \times 100 \quad (5)$$

where B1 is the sample tube, B2 the sample blank control tube, B3 the blank tube, and B4 the blank control tube.

In vitro hypoglycemic activity assay

α-amylase inhibitory activity

The α-amylase inhibitory activity was measured using the method established by Dai et al. [29], with minor adjustments. 0.1 mL of enzyme solution (2 U/mL) and 0.2 mL of polysaccharide (0.1, 0.2, 0.3, 0.4, and 0.5 mg/mL) were added to a 15 mL centrifuge tube and incubated at 37 °C for 15 min. Then, 0.2 mL of starch solution (1%) was added and incubated at 37 °C for an additional 20 min. Subsequently, 0.5 mL of 3,5-Dinitrosalicylic acid solution was added to each tube, and the tube was boiled for 15 min to terminate the reaction. Acarbose was employed as a reference standard, with each set of experiments being performed three times. Once cooled to room temperature, pipette 200 μL of each centrifuge tube's contents into a cuvette, and then the absorbance were measured at 540 nm. The α-amylase inhibition rate was calculated by following formula (6):

$$\text{Inhibition rate}(\%) = [(D1 - D2) - (D3 - D4)]/(D1 - D2) \times 100 \quad (6)$$

where D1 represents the absorbance value of the blank group, D2 the absorbance value of the blank control group, D3 the absorbance value of the polysaccharide group, and D4 the absorbance value of the sample control group.

α-glucosidase inhibitory activity

The α-glucosidase inhibitory activity of SGFP-2 was evaluated using the method described by Ren et al. [30], with minor modifications. 0.4 mL of enzyme solution (0.5 U/mL) and 0.05 mL of polysaccharide solution (0.1, 0.2, 0.3, 0.4, and 0.5 mg/mL) were added sequentially to a 15 mL centrifuge tube, and incubated at 37 °C for 15 min. Then, 0.4 mL of *p*-nitrophenyl-*α*-*D*-glucopyranoside solution was added with a concentration of 5 mmol/L and incubated at 37 °C for 30 min. Subsequently, 1 mL of Na_2CO_3 solution (1 mol/L) was added to each tube to terminate the reaction. Acarbose was employed as a reference standard, with each set of experiments being performed three times. After the experiment is stopped, pipette 200 μL of the reaction mixture from each tube into a cuvette and measure the absorbance at 405 nm using a UV–Vis spectrophotometer. The *α*-glucosidase inhibition rate was calculated using Eq. (7):

$$\text{Inhibition rate}(\%) = [(E1 - E2) - (E3 - E4)]/(E1 - E2) \times 100 \quad (7)$$

where E1 represents the absorbance value of the blank group, E2 the absorbance value of the blank control group, E3 the absorbance value of the polysaccharide group, and E4 the absorbance value of the sample control group.

Statistical analysis

All data were expressed as the mean ± standard deviation (SD). Statistical differences were calculated using one-way ANOVA with Duncan's multiple comparison test on SPSS 27.0 software, with $p < 0.05$ considered statistically significant.

Results and discussion

Isolation and purification of SGFP-2

The SGFP-2 extraction and isolation procedure is shown in Fig. 1. SGFP was successfully obtained by water extraction, ethanol precipitation, and deproteinization (Yield: 3.39%). Then, SGFP was separated on a DEAE-Crystarose Fast Flow column by elution with double-distilled water and NaCl (0.1, 0.2, and 0.3 M), and three fractions were obtained: SGFP-1 (Yield: 1.36%), SGFP-2 (Yield: 28.52%), and SGFP-3 (Yield: 10.27%). The major fraction SGFP-2 was collected and further dialyzed and lyophilized to obtain pure polysaccharides for subsequent structural characterization.

Structural characterizations analysis of SGFP-2

Molecular weight (M_w) analysis of SGFP-2

The M_w of polysaccharides has a remarkable influence on its pharmacological activity [31]. GPC chromatography results showed the M_w of SGFP-2 was 1.67×10^5 Da (Fig. 2A), which is different from the previously reported SGF1 (M_w: 621, 849 g/mol) and SGF2 (M_w: 636, 428 g/mol) [32]. Many studies have shown that the M_w should be moderate or lower for the more active polysaccharides [6]. Compared with previous studies, SGFP-2 has moderate molecular weight, which may be a favorable basis for its excellent biological activity.

FT-IR analysis of SGFP-2

The infrared spectrum information of *Siraitia grosvenorii* flower polysaccharide remains unreported to date. FT-IR spectroscopy indicated that SGFP-2 exhibits characteristic peaks typical of polysaccharides (Fig. 2B). The strong absorption peak at 3252 cm^{-1} is mainly caused by the stretching vibration of the – OH group.The peak at 2928 cm^{-1} corresponds to the stretching vibration of the C–H bond in the glycoside. Additionally, the peaks within the 1400 cm^{-1} to 1200 cm^{-1} range are identified as variable angle vibrational absorption peaks of C—H. The peak at the wavelength of 1396 cm^{-1} corresponds to the in-plane deformation vibration of O—H, and the absorption peak at 1200–1000 cm^{-1} corresponds to the C═O stretching vibration of the pyran ring. The peaks at 1140 cm^{-1}, 1070 cm^{-1}, and 1017 cm^{-1} correlate with the C—O—C versus C—O—H stretching vibrations on the pyran ring, and these peaks suggest that the sugar ring may contain pyranoside structure.

Monosaccharide compositions of SGFP-2

Monosaccharide composition analysis by HPLC showed that SGFP-2 was mainly composed of Rha, Glc, Gal, GlcA, GalA, Man, and Ara with a molar ratio of 8.17:1.54:60.06:3.41:5.37:3.54:15.44, compared with the peaks of standard monosaccharides. (Fig. 2C). Gal is one of the highest content monosaccharides in SGFP-2 composition, consistent with previous studies [32]. However, the molar ratio of monosaccharide composition in SGFP-2 differs from the other research findings [32]. It may be due to diverse origins, sources, and isolation conditions of polysaccharides, resulting in differences in monosaccharide compositions.

Methylation analysis of SGFP-2

The types of glycosidic bond connections in polysaccharide structures can be determined through methylation analysis. As shown in Table 1, GC–MS data indicated 11 identifiable glycosidic linkage patterns in SGFP-2. Methylation analysis results showed that SGFP-2 is predominantly composed of →6)-Gal*p*-(1→(30.42%), Gal*p*-(1→(22.69%), Ara*f*-(1→(18.29%), Rha*p*-(1→(8.70%), and →3,6)-Gal*p*-(1→(8.54%). Interestingly, there are various types of Gal bonds, with 1,6- and 1-bonds being the most abundant, indicating

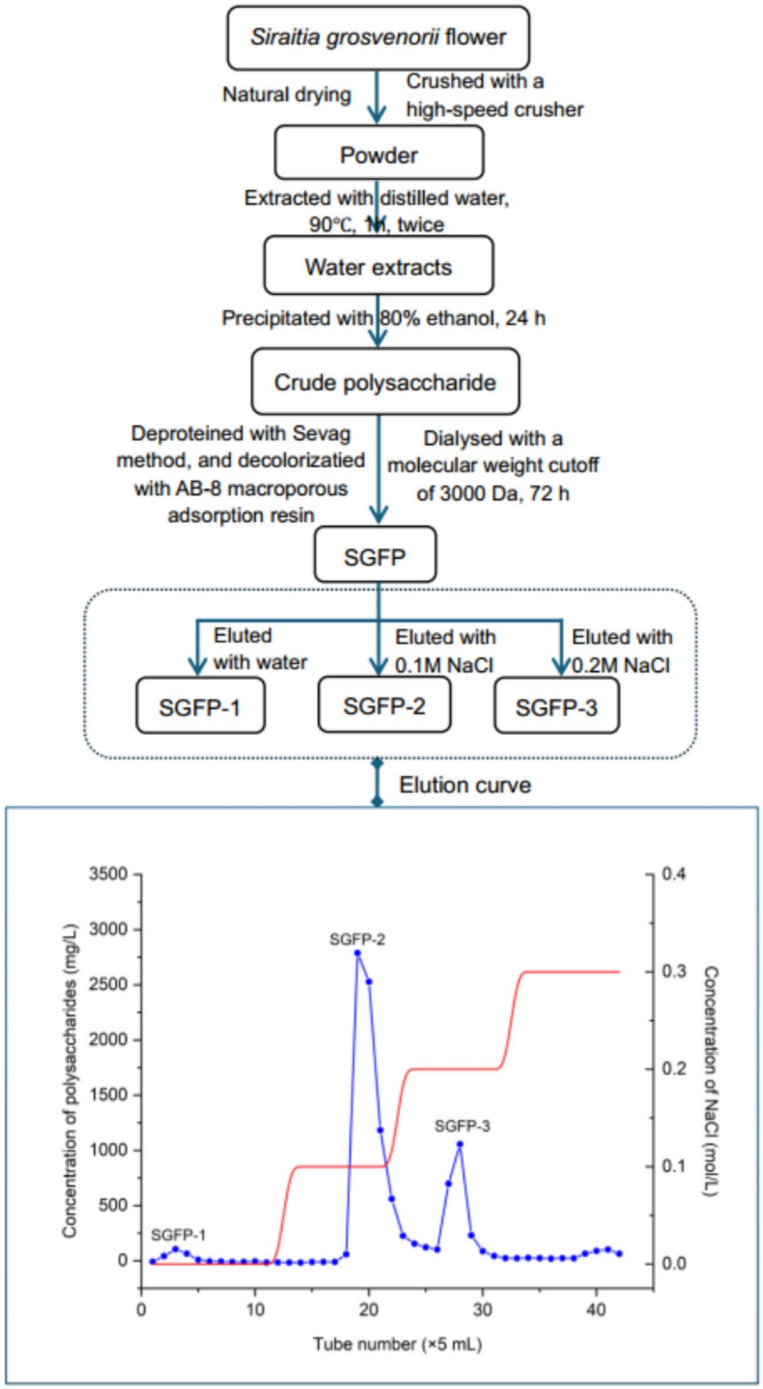


Fig. 1 Procedure of SGFP-2 extraction and isolation

that SGFP-2 is a novel polysaccharide. Many studies have demonstrated that the biological activity of polysaccharides is affected by the type and position of glycosidic bonds [33]. The revelation of the glycosidic bond type of the hypoglycemic active polysaccharide SGFP-2 provides a basis for further research on the structure–hypoglycemic activity relationship.

Congo red analysis

The complexes formed by CR with triple-helix structured polysaccharides exhibit red shifts in their

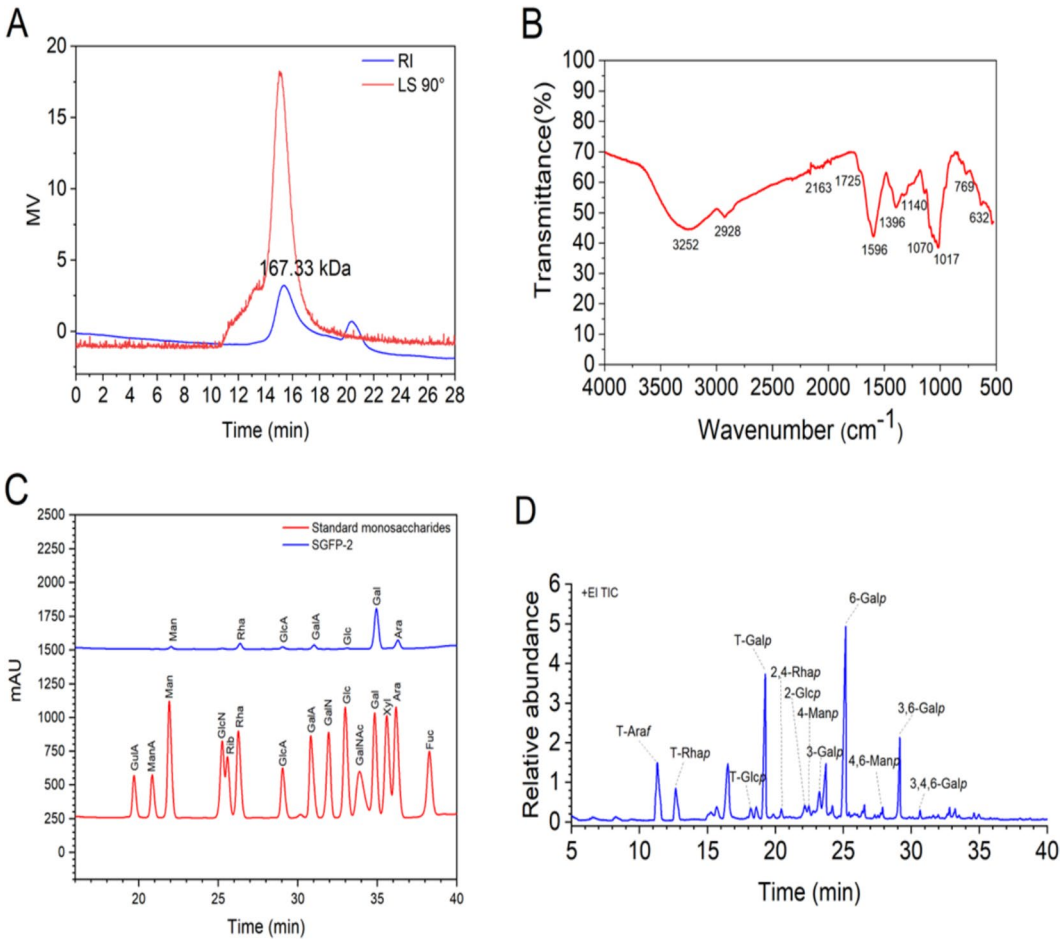


Fig. 2 Structural characterization of SGFP-2: GPC (**A**), FT-IR (**B**), monosaccharide composition (**C**), methylation (**D**)

Table 1 Methylation analysis of SGFP-2

No	PMAAs	Type of Linkage	RT (min)	Mass Fragments (m/z)	Relative Molar Ratios (%)
1	1,4-di-*O*-acetyl-1-deuterio-2,3,5-tri-*O*-methyl-D-arabinitol	Ara*f*-(1 →	11.3025	71,87,102,118,129,161	18.289
2	1,5-di-*O*-acetyl-1-deuterio-6-deoxy-2,3,4-tri-*O*-methyl-L-mannitol	Rha*p*-(1 →	12.6668	72,89,102,118,131,162	8.703
3	1,5-di-*O*-acetyl-1-deuterio-2,3,4,6-tetra-*O*-methyl-D-glucitol	Glc*p*-(1 →	18.1860	71,87,102,118,129,145,162	1.748
4	1,5-di-*O*-acetyl-1-deuterio-2,3,4,6-tetra-*O*-methyl-D-galactitol	Gal*p*-(1 →	19.2558	87,102,118,129,145,161,205	22.691
5	1,2,4,5-tetra-*O*-acetyl-1-deuterio-6-deoxy-3-*O*-methyl-L-mannitol	→ 2,4)-Rha*p*-(1 →	20.4238	71,88,101,118,130,143,190	1.126
6	1,2,5-tri-*O*-acetyl-1-deuterio-3,4,6-tri-*O*-methyl-D-glucitol	→ 2)-Glc*p*-(1 →	22.1499	71,88,101,129,161,190	1.112
7	1,3,5-tri-*O*-acetyl-1-deuterio-2,4,6-tri-*O*-methyl-D-galactitol	→ 3)-Gal*p*-(1 →	23.2248	87,101,118,129,145,161	3.585
8	1,5,6-tri-*O*-acetyl-1-deuterio-2,3,4-tri-*O*-methyl-D-galactitol	→ 6)-Gal*p*-(1 →	25.1679	87,99,118,129,162,189	30.415
9	1,4,5,6-tetra-*O*-acetyl-1-deuterio-2,3-di-*O*-methyl-D-mannitol	→ 4,6)-Man*p*-(1 →	27.8811	85,102,118,127,159,201,261	0.889
10	1,3,5,6-tetra-*O*-acetyl-1-deuterio-2,4-di-*O*-methyl-D-galactitol	→ 3,6)-Gal*p*-(1 →	29.1525	87,101,118,129,139,160,189	8.544
11	1,3,4,5,6-penta-*O*-acetyl-1-deuterio-2-*O*-methyl-D-galactitol	→ 3,4,6)-Gal*p*-(1 →	30.6409	59,97,118,129,139,160	0.699

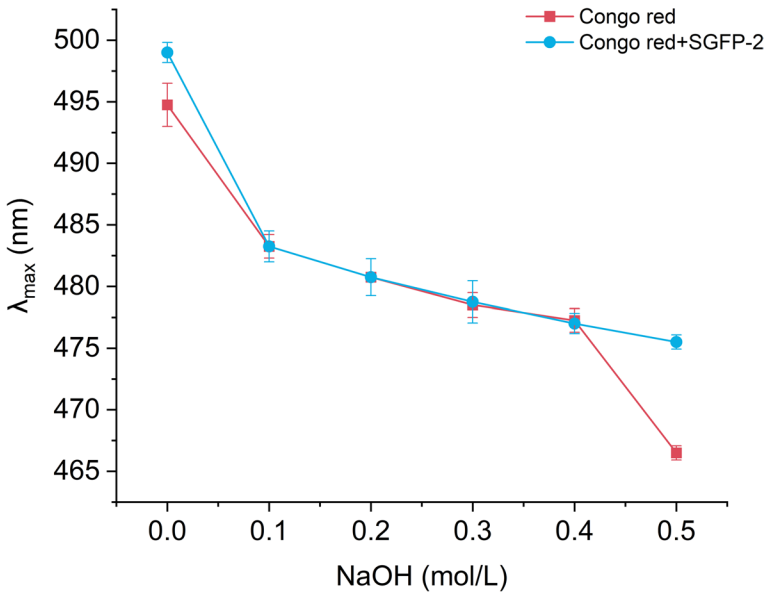


Fig. 3 The absorbance curve of Congo red and SGFP-2

maximum absorption wavelengths at suitable NaOH concentrations. Increasing the concentration of NaOH can disrupt the structure, leading to a reduction in the maximum absorption wavelength [34].

As depicted in Fig. 3, the wavelength of the maximum peak of the sample group in a weakly alkaline solution was blue-shifted compared to the CR control sample. With the increase of sodium hydroxide concentration, irregular changes occurred. The maximum absorption wavelength increased when the NaOH concentration was gradually changed to 0.5 mol/L. In a weak base solution, the maximum absorption wavelength of SGFP-2 increased as the concentration of NaOH increased. The findings proved that SGFP-2 lacked a triple-helix structure.

SEM of SGFP-2

The biological activity of polysaccharides depends on their structure and physicochemical properties [35]. The microstructure of the polysaccharide was observed using SEM, as shown in Fig. 4. SEM analysis revealed that SGFP-2 possesses distinct structural features, including a relatively smooth external surface. Its three-dimensional architecture exhibits a well-organized lamellar configuration composed of densely interwoven fibrous networks, collectively generating an exceptionally large specific surface area. The hierarchical organization of molecular components may govern key physicochemical properties including but not limited to solubility profiles, adsorption efficiency, and mass transfer dynamics. Polysaccharides with lamellar and loose structures may

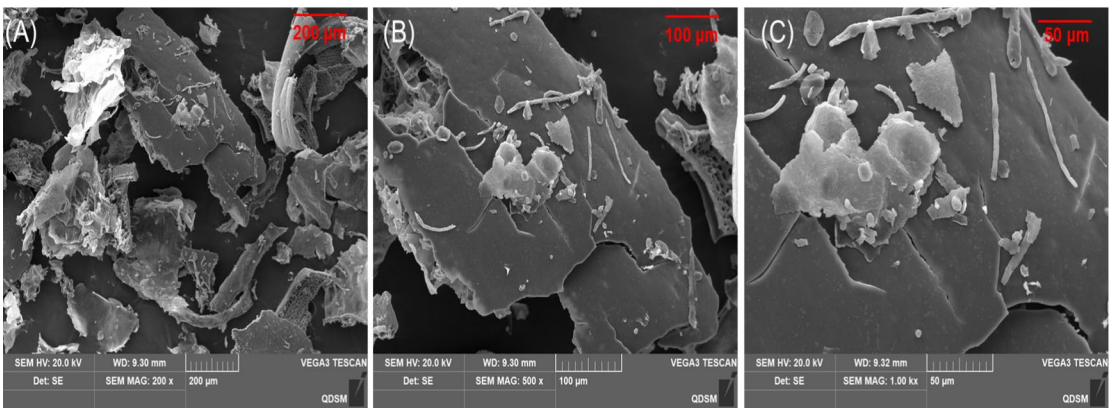


Fig. 4 SEM of SGFP-2. SGFP-2 (200×) (**A**), SGFP-2 (500×) (**B**), SGFP-2 (1000×) (**C**)

have unique spatial conformations and intermolecular interactions, affecting their binding ability with biomolecules and significantly impacting their biological activity [36, 37].

We analyzed the molecular weight, infrared spectral properties, surface morphology, monosaccharide composition, glycosidic bond types, and other key structural information of SGFP-2, which are important for our understanding of the properties of polysaccharides. However, it should be noted that the fine structure of the polysaccharide has not yet been resolved in our study. Therefore, further elucidation of the fine structure of SGFP-2 is still needed in the future to provide a reference for the study of its conformational relationship.

In vitro *analysis of hypolipidemic activities of SGFP-2*

Oil absorption capacity of SGFP-2

The oil absorption of polysaccharides is accomplished through the wrapping and adhesion of their macromolecular chains [38, 39]. The findings of the oil absorption test showed that the oil absorption capacity of SGFP-2 was 1.66 g/g. The oil absorption by SGFP-2 may be related to the porous mesh structure of its inner surface.

The adsorption of bile salts by polysaccharides

The normal body contains conjugated bile acids, which are in sodium salts, especially sodium taurocholate and sodium glycocholate. Research indicates that active compounds can inhibit the reabsorption of bile salts from the small intestine is reduced, resulting in increased excretion of bile salts in feces. This occurs through the binding of these compounds to bile salts, resulting in a

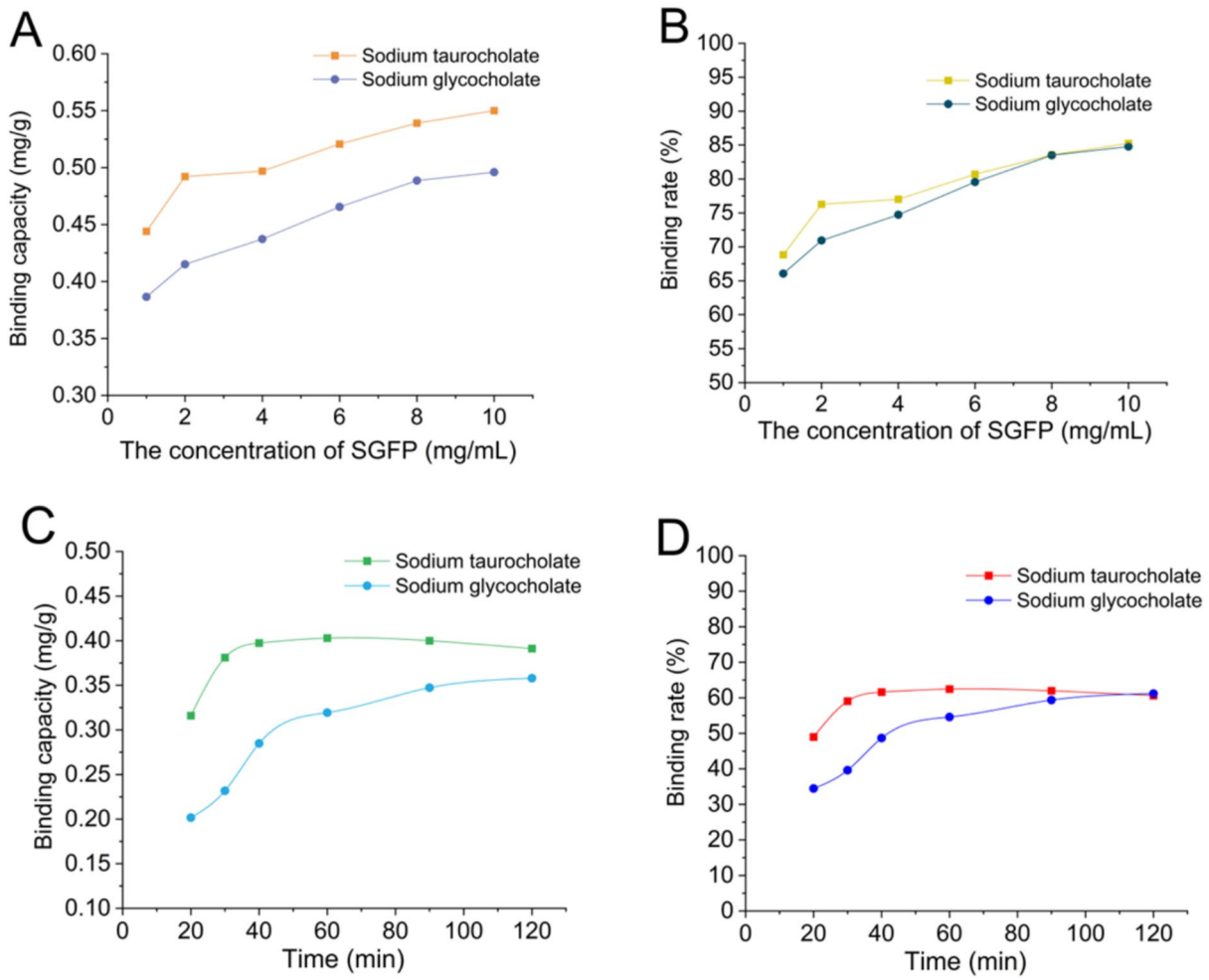


Fig. 5 In vitro adsorption capacity and adsorption kinetics of bile salts by SGFP-2. Cholate binding capacity (**A**), Cholate binding ratio (**B**), Kinetic curves of cholate adsorption at different times (**C**) and (**D**)

reduction of blood lipid levels [40, 41]. Polysaccharide-based biosorbents effectively diminish excess bile salts in the gastrointestinal tract and address cardiovascular disorders [42]. Figure 5 illustrates the adsorption effect of SGFP-2 on bile salts. The adsorption capacities of SGFP-2 for sodium taurocholate and sodium glycylcholate increased with higher concentrations ranging from 1 to 10 mg/mL. Notably, at a concentration of 10 mg/mL, SGFP-2 achieves peak binding rates of 85.26% for sodium taurocholate (Fig. 5A) and 84.78% for sodium glycocholate (Fig. 5B), corresponding to maximum binding capacities of 0.550 mg/g and 0.496 mg/g, respectively.

The experiments on bile salt adsorption demonstrated that polysaccharides from *Siraitia grosvenorii* flowers exhibit effective binding to sodium glycocholate and sodium taurocholate, achieving maximum binding capacities of 0.358 mg/g and 0.391 mg/g, respectively (Fig. 5C). The binding affinity of SGFP-2 for sodium taurocholate and sodium glycocholate increases progressively over time until it reaches a plateau. The binding of the polysaccharide to sodium taurocholate attains its peak rate of 62.41% within 60 min across the tested range. Similarly, the binding of the polysaccharide to sodium glycylcholate reaches a maximum of 61.21% after 120 min (Fig. 5D). These observations suggest that SGFP-2 can effectively interact with bile salts under conditions that mimic the in vivo environment. These findings indicated that SGFP-2 has potential lipid-lowering properties, potentially enhancing the metabolic rate of cholesterol within the body and thus reducing cholesterol accumulation.

The inhibition of cholesterol esterase and pancreatic lipase activities

Numerous studies have shown that inhibiting pancreatic lipase and cholesterol esterase activity is an effective strategy for lowering blood lipids and ameliorating metabolic diseases such as obesity and hyperlipidemia [43, 44]. Polysaccharides have been proven to act as

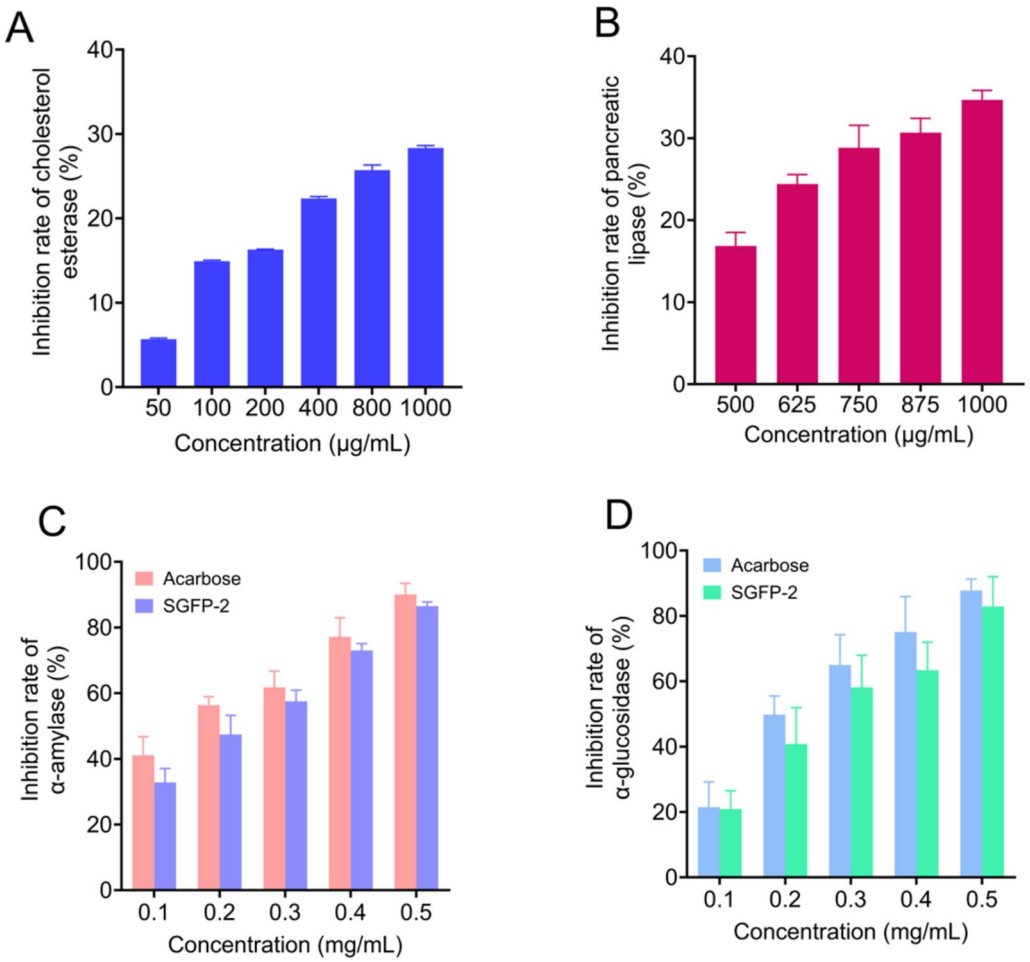


Fig. 6 In vitro enzyme activity inhibition of SGFP-2. Cholesterol lipase (**A**), Pancreatic lipase (**B**), *α*-amylase (**C**), *α*-glucosidase (**D**)

natural enzyme inhibitors, effectively inhibiting the activity of lipase, and thus showing lipid-lowering effects [45, 46]. Figure 6 illustrates that the inhibitory effects of SGFP-2 on cholesterol esterase and pancreatic lipase progressively increased with increasing polysaccharide concentration within the experimental range, indicating a dose–response relationship between the inhibitory effects on the two enzymes. SGFP-2 inhibited cholesterol esterase and pancreatic lipase by 28.57% (Fig. 6A) and 34.67% (Fig. 6B), respectively, at a 1.0 mg/mL polysaccharide concentration. The inhibitory effect of SGFP-2 on pancreatic lipase was comparable to that of polysaccharide extracted from *Laminaria japonica* [47], but both were lower than that of polysaccharide from *Bangia fusco-purpurea* [46]. The differences in the inhibitory effects of different polysaccharide fractions on pancreatic lipase may be attributed to the effects of the monosaccharide composition, glycosidic bonding, molecular weight and chain conformation of polysaccharides. SGFP-2 has a highly reticular structure with a porous interior, which may favor polysaccharide-enzyme interactions and thus inhibit cholesterol esterase and pancreatic lipase. These results indicated that *Siraitia grosvenorii* flower polysaccharides have potential hypolipidemic effects in vitro.

In vitro analysis of hypoglycemic activities of SGFP-2

α-Amylase and *α*-glucosidase facilitate the decomposition of starch and oligosaccharides into glucose and are essential enzymes in digestion [48]. These enzymes serve as viable therapeutic targets for managing type 2 diabetes and obesity [49]. The in vitro hypoglycemic efficacy of *Siraitia grosvenorii* floral polysaccharides was measured by *α*-amylase and *α*-glucosidase inhibition tests. As shown in Fig. 6C and D, SGFP-2 greatly inhibited *α*-amylase and *α*-glucosidase, and both inhibitions were significantly concentration-dependent. At a concentration of 0.5 mg/mL, SGFP-2 exhibited a significant inhibitory effect on the activities of α-amylase and α-glucosidase, with inhibition rates of 85.84% and 82.79%, respectively.

The inhibitory activities of α-glucosidase and α-amylase are highly correlated with the monosaccharide composition, molecular weight, types of glycosyl linkage and spatial conformation of polysaccharides [50–52]. Some studies have shown that polysaccharides containing more galactose residues, especially those with glycosyl linkage of (1 → 6)-α-D-galactose, have more effective α-glucosidase and α-amylase inhibitory activities. The inhibitory effect of SGFP-2 on α-amylase was stronger than blue honeysuckle berries polysaccharide [53] and *Hippophae rhamnoide* L. polysaccharides [51]. Besides, the inhibitory effect of SGFP-2 on α-glucosidase was stronger than *Camellia oleifera* Abel polysaccharides [54] and *Magnolia officinalis* flowers' polysaccharides [55]. These findings suggest that SGFP-2 is a natural bioactive α-amylase and α-glucosidase inhibitor with potential for the development of dietary supplement ingredient.

While the current findings provide valuable insights into the biofunctional properties of SGFP-2, the absence of cellular absorption dynamics and in vivo validation models precludes direct extrapolation to physiological contexts. Subsequent investigations should prioritize establishing structure–activity relationships through integrated approaches combining metabolomic profiling with preclinical evaluations in diet-induced metabolic syndrome models.

Conclusions

This study successfully isolated SGFP-2, a heteropolysaccharide from *Siraitia grosvenorii* flowers, with a molecular weight of 1.67×10^5 Da. Structural analysis identified that SGFP-2 is mainly composed of Rha, Glc, Gal, GlcA, GalA, Man, and Ara with a molar ratio of 8.17:1.54:60.06:3.41:5.37:3.54:15.44. The major types of glycosidic bond of SGFP-2 consists of → 6)-Galp-(1 → (30.42%), Galp-(1 → (22.69%), Araf-(1 → (18.29%), Rhap-(1 → (8.70%), → 3,6)-Galp-(1 → (8.54%), differing from previously reported polysaccharides in *S. grosvenorii* flowers. Morphological characterization revealed that the network structure of SGFP-2 was lamellar without trihelix conformation. In vitro evaluation demonstrated dose-dependent lipid/bile salt adsorption capacities and multitarget enzymatic inhibition, suggesting dual modulatory potential on lipid-glucose homeostasis. These findings suggest that *S. grosvenorii* flowers polysaccharides have potential hypolipidemic and hypoglycemic activities. Further validation and revelation of its biological activities through more systematic in vivo and in vitro experiments are needed in the future to facilitate the development and utilization of its functional products.

Abbreviations

Ara	Arabinose
Ara*f*	Arabinopyranosyl
DEAE	Diethyl aminoethyl
FT-IR	Fourier transform infrared spectroscopy
Gal	Galactose
Gal*p*	Galactopyranosyl
GalA	Galacturonic acid
Glc	Glucose
GlcA	Glucuronic acid
Glc*p*	Glucopyranosyl
GC	Gas chromatography
GC–MS	Gas chromatography-mass spectrometer
GPC	Gel permeation chromatography
HPLC	High-performance liquid chromatography
IR	Infrared spectroscopy
Man	Mannose
Man*p*	Mannopyranosyl

MW	Average molecular weight
NMR	Nuclear magnetic resonance
PD	Polydispersity
Rha	Rhamnose
Rha*p*	Rhamnopyranosyl
Rib	Ribose
SEM	Scanning electron microscopy
UV	Ultraviolet and visible spectrum
Xyl	Xylose
Xyl*p*	Xylopyranosyl

Acknowledgements
This work was supported by the Natural Science Foundation of Guangxi Province of China (No. 2023GXNSFBA026322), Key R&D Program of the Guangxi Zhuang Autonomous Region (No. AB19110023).

Author contributions
Hao Teng: Writing—original draft, Formal analysis, Investigation, Conceptualization, Writing—review & editing, Project administration. Limei Qiu: Formal analysis, Investigation. Zhizhi Huang: Formal analysis, Investigation. Sam Al-Dalali: Writing—review & editing, Supervision. Cailin Li: Formal analysis, Validation. Aiying Xu: Investigation. Zhigui He: Writing—review & editing, Supervision, Project administration.

Data availability
No datasets were generated or analyzed during the current study.

Declarations

Competing interests
The authors declare no competing interests.

Author details
[1]School of Food and Health, Guilin Tourism University, Guilin 541006, China. [2]Guangxi Engineering Research Center for Large-Scale Preparation & Nutrients and Hygiene of Guangxi Cuisine, Guilin 541006, China. [3]Key Laboratory of Industrialized Processing and Safety of Guangxi Cuisine, Education Department of Guangxi Zhuang Autonomous Region, Guilin Tourism University, Nanning, China.

Received: 18 January 2025 Accepted: 18 February 2025
Published online: 06 March 2025

References

1. Vergès B. Pathophysiology of diabetic dyslipidaemia: where are we? Diabetologia. 2015;58:886–99. https://doi.org/10.1007/s00125-015-3525-8.
2. Opazo-Ríos L, Mas S, Marín-Royo G, Mezzano S, Gómez-Guerrero C, Moreno JA, et al. Lipotoxicity and diabetic nephropathy: novel mechanistic insights and therapeutic opportunities. Int J Mol Sci. 2020;21(7):2632. https://doi.org/10.3390/ijms21072632.
3. Turer CB, Brady TM, De Ferranti SD. Obesity, hypertension, and dyslipidemia in childhood are key modifiable antecedents of adult cardiovascular disease: a call to action. Circulation. 2018;137:1256–9. https://doi.org/10.1161/CIRCULATIONAHA.118.032531.
4. Moosmann B, Behl C. Selenoprotein synthesis and side-effects of statins. Lancet. 2004;363(9412):892–4. https://doi.org/10.1016/S0140-6736(04)15739-5.
5. Huang T, Wu T, Wu YD, Li XH, Tan J, Shen CH, et al. Long-term statins administration exacerbates diabetic nephropathy via ectopic fat deposition in diabetic mice. Nat Commun. 2023;14(1):390. https://doi.org/10.1038/s41467-023-35944-z.
6. Ji X, Guo J, Cao T, Zhang T, Liu Y, Yan Y. Review on mechanisms and structure-activity relationship of hypoglycemic effects of polysaccharides from natural resources. Food Sci Hum Wellness. 2023;12:1969–80. https://doi.org/10.1016/j.fshw.2023.03.017.
7. Tang C, Wang YX, Chen D, Zhang M, Xu J, Xu C, et al. Natural polysaccharides protect against diet-induced obesity by improving lipid metabolism and regulating the immune system. Food Res Int. 2023;172:113192. https://doi.org/10.1016/j.foodres.2023.113192.
8. Wang T, Han J, Dai H, Sun J, Ren J, Wang W, et al. Polysaccharides from Lyophyllum decastes reduce obesity by altering gut microbiota and increasing energy expenditure. Carbohydr Polym. 2022;295: 119862. https://doi.org/10.1016/j.carbpol.2022.119862.
9. Chen D, Wang A, Lv J, Peng Y, Zheng Y, Zuo J, et al. Tea (*Camellia sinensis* L.) flower polysaccharide attenuates metabolic syndrome in high-fat diet induced mice in association with modulation of gut microbiota. Int J Biol Macromol. 2024;279: 135340. https://doi.org/10.1016/j.ijbiomac.2024.135340.
10. Zhao X, Fu X, Wang T, Xu R, Shayiranbieke A, Zheng X, et al. Screening of bioactive flavour compounds targeting muscarinic-3 acetylcholine receptor from *Siraitia grosvenorii* and evaluation of their synergistic anti-asthmatic activity. Food Chem. 2022;395: 133593. https://doi.org/10.1016/j.foodchem.2022.133593.
11. Abdel-Hamid M, Romeih E, Huang Z, Enomoto T, Huang L, Li L. Bioactive properties of probiotic set-yogurt supplemented with *Siraitia grosvenorii* fruit extract. Food Chem. 2020;303: 125400. https://doi.org/10.1016/j.foodchem.2019.125400.
12. Mo LL, Li DP. Antioxidant activity of flavonol glycosides of *Siraitia Grosvenorii* flower. Mod Food Sci Technol. 2009;25(5):484–6. https://doi.org/10.13982/j.mfst.1673-9078.2009.05.029.
13. Xu Y, Zhao L, Chen L, Du Y, Lu Y, Luo C, et al. Selective enzymatic α-1,6- monoglucosylation of mogroside IIIE for the bio-creation of α-siamenoside I, a potential high-intensity sweetener. Food Chem. 2021;359: 129938. https://doi.org/10.1016/j.foodchem.2021.129938.
14. Zhu YM, Pan LC, Zhang LJ, Yin Y, Zhu ZY, Sun HQ, et al. Chemical structure and antioxidant activity of a polysaccharide from *Siraitia grosvenorii*. Int J Biol Macromol. 2020;165:1900–10. https://doi.org/10.1016/j.ijbiomac.2020.10.127.
15. Gong P, Cui D, Guo Y, Wang M, Wang Z, Huang Z, et al. A novel polysaccharide obtained from: *Siraitia grosvenorii* alleviates inflammatory responses in a diabetic nephropathy mouse model via the TLR4-NF-κB pathway. Food Funct. 2021;12(19):9054–65. https://doi.org/10.1039/d1fo01182k.
16. Sung YY, Kim SH, Yuk HJ, Yang WK, Lee YM, Son E, et al. *Siraitia grosvenorii* residual extract attenuates ovalbumin-induced lung inflammation by down-regulating IL-4, IL-5, IL-13, IL-17, and MUC5AC expression in mice. Phytomedicine. 2019;61: 152835. https://doi.org/10.1016/j.phymed.2019.152835.
17. Thakur K, Partap M, Kumar P, Sharma R, Warghat AR. Understandings of bioactive composition, molecular regulation, and biotechnological interventions in the development and usage of specialized metabolites as health-promoting substances in *Siraitia grosvenorii* (Swingle) C. Jeffrey. J Food Compos Anal. 2023;116: 105070. https://doi.org/10.1016/j.jfca.2022.105070.
18. Kang W, Meng L, Wang L, Qu J, Liu L, Li C. Chemical composition and biological activity of polysaccharides from flowers: a review. Food Sci. 2022;43(01):1–13. https://doi.org/10.7506/spkx1002-6630-20210813-176.
19. Teng H, He Z, Li X, Shen W, Wang J, Zhao D, et al. Chemical structure, antioxidant and anti-inflammatory activities of two novel pectin polysaccharides from purple passion fruit (*Passiflora edulia* Sims) peel. J Mol Struct. 2022;1264: 133309. https://doi.org/10.1016/j.molstruc.2022.133309.
20. Han Z, Zeng Y, Zhang M, Zhang Y, Zhang L. Monosaccharide compositions of sulfated chitosans obtained by analysis of nitrous acid degraded and pyrazolone-labeled products. Carbohydr Polym. 2016;136:376–83. https://doi.org/10.1016/j.carbpol.2015.07.087.
21. Ernst L, Werner A, Wefers D. Influence of ultrasonication and hydrolysis conditions in methylation analysis of bacterial homoexopolysaccharides. Carbohydr Polym. 2023;308: 120643. https://doi.org/10.1016/j.carbpol.2023.120643.
22. Li H, Gao T, Zhang Z, Lei J, Hu J, Tang Z, et al. A novel Stauntonia leucantha fruits arabinogalactan: and structural characterization. Carbohydr Polym. 2023;303: 120481. https://doi.org/10.1016/j.carbpol.2022.120481.
23. Wu D, Tang L, Zeng Z, Zhang J, Hu X, Pan Q, et al. Delivery of hyperoside by using a soybean protein isolated-soy soluble polysaccharide nanocomplex: fabrication, characterization, and in vitro release

properties. Food Chem. 2022;386: 132837. https://doi.org/10.1016/j.foodchem.2022.132837.
24. Ji X, Cheng Y, Tian J, Zhang S, Jing Y, Shi M. Structural characterization of polysaccharide from jujube (*Ziziphus jujuba* Mill.) fruit. Chem Biol Technol Ag. 2021;8(1):54. https://doi.org/10.1186/s40538-021-00255-2.
25. Hu T, Cai W, Cai W, Zheng Z, Xiao Y, Huang Q. Structure, size and aggregated morphology of a β-D-glucan from *Lignosus rhinocerotis* as affected by ultrasound. Carbohydr Polym. 2021;269: 118344. https://doi.org/10.1016/j.carbpol.2021.118344.
26. Yang W, Wu J, Liu W, Ai Z, Cheng Y, Wei Z, et al. Structural characterization, antioxidant and hypolipidemic activity of *Grifola frondosa* polysaccharides in novel submerged cultivation. Food Biosci. 2021;42: 101187. https://doi.org/10.1016/j.fbio.2021.101187.
27. Chu J, Zhao H, Lu Z, Lu F, Bie X, Zhang C. Improved physicochemical and functional properties of dietary fiber from millet bran fermented by *Bacillus natto*. Food Chem. 2019;294:79–86. https://doi.org/10.1016/j.foodchem.2019.05.035.
28. Long X, Hu X, Xiang H, Chen S, Li L, Qi B, et al. Structural characterization and hypolipidemic activity of *Gracilaria lemaneiformis* polysaccharide and its degradation products. Food Chem X. 2022;14: 100314. https://doi.org/10.1016/j.fochx.2022.100314.
29. Dai Y, He Y, Ma Y, Yang X, Huang Y, Min H, Liu X. Purification, structural analysis, and hypoglycemic activity of *Auricularia auricula-judae* polysaccharides extracted with natural deep eutectic solvents. J Funct Foods. 2024;122: 106524. https://doi.org/10.1016/j.jff.2024.106524.
30. Ren Y, Zhu Z, Sun H, Chen L. Structural characterization and inhibition on α-glucosidase activity of acidic polysaccharide from *Annona squamosa*. Carbohydr Polym. 2017;174:1–12. https://doi.org/10.1016/j.carbpol.2017.05.092.
31. Teng H, He Z, Hong C, Xie S, Zha X. Extraction, purification, structural characterization and pharmacological activities of polysaccharides from sea buckthorn (*Hippophae rhamnoides* L.): a review. J Ethnopharmacol. 2024;324:117809. https://doi.org/10.1016/j.jep.2024.117809.
32. Dujnič V, Matulová M, Chyba A, Pätoprstý V. Polysaccharides in *Siraitia grosvenori* flowers and herbal tea. Chem Pap. 2021;75(3):1175–85. https://doi.org/10.1007/s11696-020-01347-3.
33. Zhang R, Zhang X, Tang Y, Mao J. Composition, isolation, purification and biological activities of *Sargassum fusiforme* polysaccharides: a review. Carbohydr Polym. 2022;228: 115381. https://doi.org/10.1016/j.carbpol.2019.115381.
34. Yang X, Dai J, Zhong Y, Wei X, Wu M, Zhang Y, et al. Characterization of insoluble dietary fiber from three food sources and their potential hypoglycemic and hypolipidemic effects. Food Funct. 2021;12(14):6576–87. https://doi.org/10.1039/d1fo00521a.
35. Fu Y, Jiao H, Sun J, Okoye CO, Zhang H, Li Y, et al. Structure-activity relationships of bioactive polysaccharides extracted from macroalgae towards biomedical application: a review. Carbohydr Polym. 2024;324: 121533. https://doi.org/10.1016/j.carbpol.2023.121533.
36. Falsafi SR, Rostamabadi H, Samborska K, Mirarab S, Rashidinejhad A, Jafari SM. Protein-polysaccharide interactions for the fabrication of bioactive-loaded nanocarriers: chemical conjugates and physical complexes. Pharmacol Res. 2022;178: 106164. https://doi.org/10.1016/j.phrs.2022.106164.
37. Ji XL, Guo JH, Tian JY, Ma K, Liu YQ. Research progress on degradation methods and product properties of plant polysaccharides. J Light Ind. 2023;38(3):55–62. https://doi.org/10.12187/2023.03.007.
38. Shao M, Li S, Huang S, Junejo SA, Jiang Y, Zhang B, et al. Oil structuring from porous starch to powdered oil: role of multi-scale structure in the oil adsorption and distribution. Int J Biol Macromol. 2023;253: 126968. https://doi.org/10.1016/j.ijbiomac.2023.126968.
39. Qu D, Wang S, Zhao H, Liu H, Zhu D, Jiang L. Structure and interfacial adsorption behavior of soy hull polysaccharide at the oil/water interface as influenced by pH. Food Hydrocoll. 2021;116: 106638. https://doi.org/10.1016/j.foodhyd.2021.106638.
40. Liu X, Sun Z, Zhang M, Meng X, Xia X, Yuan W, et al. Antioxidant and antihyperlipidemic activities of polysaccharides from sea cucumber *Apostichopus japonicus*. Carbohydr Polym. 2012;90(4):1664–70. https://doi.org/10.1016/j.carbpol.2012.07.047.
41. Gunness P, Gidley MJ. Mechanisms underlying the cholesterol-lowering properties of soluble dietary fibre polysaccharides. Food Funct. 2010;1:149–55. https://doi.org/10.1039/c0fo00080a.
42. Chen L, He X, Pu Y, Cao J, Jiang W. Polysaccharide-based biosorbents for cholesterol and bile salts in gastric-intestinal passage: advances and future trends. Compr Rev Food Sci Food Saf. 2023;22:3790–813. https://doi.org/10.1111/1541-4337.13214.
43. Nomura DK, Casida JE. Lipases and their inhibitors in health and disease. Chem Biol Interact. 2016;259:211–22. https://doi.org/10.1016/j.cbi.2016.04.004.
44. He X, Chen L, Pu Y, Wang H, Cao J, Jiang W. Fruit and vegetable polyphenols as natural bioactive inhibitors of pancreatic lipase and cholesterol esterase: inhibition mechanisms, polyphenol influences, application challenges. Food Biosci. 2023;55: 103054. https://doi.org/10.1016/j.fbio.2023.103054.
45. Xu L, Pan X, Li D, Wang Z, Tan L, Chang M, et al. Structural characterization, rheological characterization, hypoglycemic and hypolipidemic activities of polysaccharides from Morchella importuna using acidic and alkaline deep eutectic solvents. LWT-Food Sci Technol. 2024;193: 115742. https://doi.org/10.1016/j.lwt.2024.115742.
46. Zheng M, Ouyang H, Li Z, Hong T, Zhu Y, Yang Y, et al. Ultra-high pressure assisted extraction of polysaccharide from *Bangia fusco-purpurea*: structure and in vitro hypolipidemic activity. Int J Biol Macromol. 2024;280: 135687. https://doi.org/10.1016/j.ijbiomac.2024.135687.
47. Zhang T, Wu S, Ai C, Wen C, Liu Z, Wang L, et al. Galactofucan from *Laminaria japonica* is not degraded by the human digestive system but inhibits pancreatic lipase and modifies the intestinal microbiota. Int J Biol Macromol. 2021;166:611–20. https://doi.org/10.1016/j.ijbiomac.2020.10.219.
48. Aleixandre A, Gil JV, Sineiro J, Rosell CM. Understanding phenolic acids inhibition of α-amylase and α-glucosidase and influence of reaction conditions. Food Chem. 2022;372: 131231. https://doi.org/10.1016/j.foodchem.2021.131231.
49. Rasouli H, Hosseini-Ghazvini S, Adibi H, Khodarahmi R. Differential α-amylase/α-glucosidase inhibitory activities of plant-derived phenolic compounds: a virtual screening perspective for the treatment of obesity and diabetes. Food Funct. 2017;8(5):1942–54. https://doi.org/10.1039/c7fo00220c.
50. Hu T, Wu P, Zhan J, Wang W, Shen J, Wang M, et al. Structure variety and its potential effects on biological activity of tea polysaccharides. Food Sci Hum Wellness. 2022;11:587–97. https://doi.org/10.1016/j.fshw.2021.12.015.
51. Yang Y, Li M, Sun J, Qin S, Diao T, Bai J, et al. Microwave-assisted aqueous two-phase extraction of polysaccharides from *Hippophae rhamnoide* L.: Modeling, characterization and hypoglycemic activity. Int J Biol Macromol. 2024;254:127626. https://doi.org/10.1016/j.ijbiomac.2023.127626.
52. An K, Wu J, Xiao H, Hu T, Yu Y, Yang W, et al. Effect of various drying methods on the physicochemical characterizations, antioxidant activities and hypoglycemic activities of lychee (*Litchi chinensis* Sonn.) pulp polysaccharides. Int J Biol Macromol. 2022;220:510–9. https://doi.org/10.1016/j.ijbiomac.2022.08.083.
53. Fu X, Yang H, Ma C, Li X, Li D, Yang Y, et al. Characterization and inhibitory activities on α-amylase and α-glucosidase of the polysaccharide from blue honeysuckle berries. Int J Biol Macromol. 2020;163:414–22. https://doi.org/10.1016/j.ijbiomac.2020.06.267.
54. Zhang S, Li XZ. Inhibition of α-glucosidase by polysaccharides from the fruit hull of *Camellia oleifera* Abel. Carbohydr Polym. 2015;115:38–43. https://doi.org/10.1016/j.carbpol.2014.08.059.
55. Hao K, Zhong R, Zhang J, Shen C, Xu X, Jiang J. Comparison of polysaccharides from stem barks and flowers of Magnolia officinalis: compositional characterization, hypoglycemic and photoprotection activities. Int J Biol Macromol. 2024;283: 137766. https://doi.org/10.1016/j.ijbiomac.2024.137766.

Publisher's Note

Springer Nature remains neutral with regard to jurisdictional claims in published maps and institutional affiliations.